IEEE Access
Multidisciplinary | Rapid Review | Open Access Journal

Received August 12, 2019, accepted September 23, 2019, date of publication September 26, 2019, date of current version October 9, 2019.

Digital Object Identifier 10.1109/ACCESS.2019.2943880

A Compact Circularly Polarized MIMO Dielectric Resonator Antenna Over Electromagnetic Band-Gap Surface for 5G Applications

HSIANG NERNG CHEN, JEONG-MOON SONG, AND JUNG-DONG PARK, (Senior Member, IEEE)
Division of Electronics and Electrical Engineering, Dongguk University, Seoul 04620, South Korea

Corresponding author: Jung-Dong Park (jdpark@dongguk.edu)

This work was supported in part by the National Research Foundation of Korea (NRF) Grant funded by the Korean Government (MSIP) under Grant 2018R1C1B5045481, in part by the Korea Institute of Energy Technology Evaluation and Planning (KETEP), and in part by the Ministry of Trade, Industry and Energy (MOTIE) of South Korea under Grant 20194030202320.

ABSTRACT We present a wideband circularly polarized (CP) multiple-input multiple-output (MIMO) dielectric resonator antenna (DRA) with enhanced diversity. In the DRA element, two diagonal edges of the DR were truncated at 45° to obtain a wider axial ratio larger than 0.65 GHz. The DRA element was excited by a cross-ring slot with specific slot-arm ratio through microstrip-line (MSTL) implemented at the backside of the FR4 substrate to generate CP fields. Small triangular stands at the edge of the DR were employed to hold it in place to avoid any degradation from the uncontrollable bonding agent used for attaching DR onto the FR4 substrate. The DRA achieved an impedance bandwidth better than 0.8 GHz with an antenna gain of 4.83 dBi. Using the DRA with the MSTL feed, two-element CP-DRA array was implemented with electromagnetic band-gap (EBG) structure etched onto the ground plane of the MSTL. The proposed architecture achieves isolation better than 26 dB over the desired frequency band without any performance degradation while maintaining its compact size in the array. Various diversity analysis was carried out on the implemented circularly polarized MIMO DRA. The measured results demonstrated that the proposed singly fed DRA with EBG on the ground plate is suitable for implementing wideband circular polarized MIMO antennas in a compact size.

INDEX TERMS Dielectric resonator antennas, electromagnetic band-gap, MIMO, mutual coupling.

I. INTRODUCTION

Nearly four decades ago, the investigation on dielectric resonator antenna (DRA) performed by Long *et al.* [1] has drawn significant attention due to a number of attractive features, such as low profile, high radiation efficiency, wide bandwidth and ease of excitation [2]–[4]. Linear polarized (LP) DRAs have been studied extensively up until the early 2000s. However, there have been few reports on circularly polarized (CP) DRAs [5], [6]. [7]; these are generally preferred due to their enhanced immunity toward antenna misalignment and propagation effects [5]. Multi-feed structures have been reported to increase the axial ratio (AR) bandwidth of a CP-DRA at the expense of requiring an external power divider or quadrature coupler, thereby increasing the system size and complexity [6], [7].

As compact wideband systems are in high demand in modern wireless communication, numerous methods for single point fed designs have been explored to date. Different shapes of CP-DRAs aimed at wider AR bandwidth have been reported, such as stair-shape [8], DR with outer-fed square spiral strip [9], hollow DR [10], a slotted DR with parasitic strips [11], and DR with inclined slots [12], [13]. Slot excitation methods on the DR, with dual-resonance and broadband characteristics, which is first introduced by Buerkle *et al.* [14] has been widely used for the fabrication simplicity, low-cross polarization levels, and non-negligible back radiation advantages. The said method has then been further utilized in [15]–[17], which consists of dual-band and broadband circularly polarized operations, aiming at GPS & WLAN applications. Other recent slot design techniques for CP

The associate editor coordinating the review of this manuscript and approving it for publication was Mohsen Khalily.

involved are the logarithmic spiral slot [18] and plus-shaped slot [19]. However, there has not been many investigations on truncation or partially truncated DRA with the slot structures for wideband CP applications in the S-band frequency range.

Upon using a DR in a compact antenna, bonding agents are typically applied to the surface between the DR and the substrate. This results in significant performance degradation of the DRA as the use of adhesives causes distinctive variation in the radiation characteristics [20], [21]. In [20], the spin coating was used on the edges of the circular DR and substrate, incurring additional machinery cost. Although no adhesive was used in [21], a strategic hole was cut into a second ground plane to accommodate the DR with two metal holder pins soldered beside the hole for accurate positioning, increasing the fabrication complexity to a certain degree. In this regard, there has not yet been an efficient design to avoid this issue.

In recent years, multiple-input multiple-output (MIMO) technologies have been in constant development for modern telecommunication systems. MIMO antenna systems are known to be used for wireless local networks (WLANs), long-term evolution (LTE), and possibly fifth-generation (5G) communication. The demand for compact MIMO antennas arises to facilitate mobile terminals and base stations for space-saving and aesthetic purposes [22]. One of the critical considerations in designing a MIMO antenna system is by having low mutual coupling among the radiating elements. MIMO antennas designed through patch antennas tend to have lower efficiencies and insufficient isolation between unit antennas, which renders it unsuitable in most applications [23]. To combat the issue, a compact DRAs possessing high radiation efficiency will be much more favorable, observing no unwanted effects even in array configurations with better isolation.

Numerous works on reducing mutual coupling between DRA elements have been reported. Defected ground plane structures (DGS) draws attention by manipulating the surface waves, reducing mutual coupling. A fractal DRA and defected ground structures (DGS) was implemented with isolation has enhanced up to 15 dB [24]. Similarly, Maltese-shaped DRAs utilizing C-shaped periodic DGS observes a significant reduction in mutual coupling [25]. There are several electromagnetic band-gap (EBG) structure designs have been incorporated in DRAs as well. One design achieved a 13 dB isolation with the use of EBG [26]. Meta-surface shield in the configuration of side split-ring resonators (SRR) shown a reduction in the mutual coupling, however, at a much higher frequency and with the expense of radiation pattern degradation [27]. In another related research, a metamaterial polarization-rotator wall (MPR) between cylindrical DRAs have been implemented, resulting in a 16 dB reduction in mutual coupling [28].

Nevertheless, the above-mentioned previous works are linearly polarized and subject to performance degradation in case of misalignment [29]. As of date, there are little to no significant work performed on circularly polarized

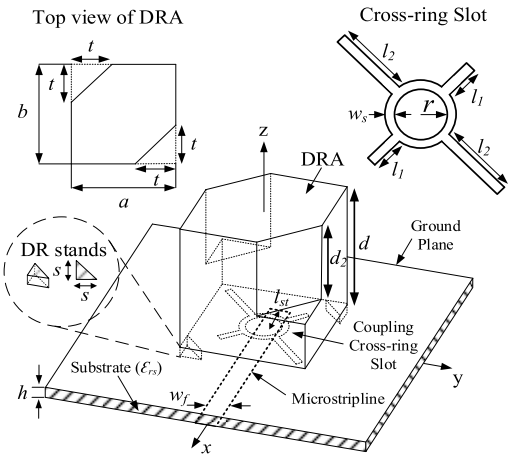

FIGURE 1. Geometry of the proposed CP-DR.

MIMO DRAs, except for a few recorded works to overcome misalignment difficulties and focuses on multi-band operations [29]–[32]. An efficient mutual coupling reduction hybrid technique has been proposed in [33] for a wideband circular polarized MIMO DRA. However, the diagonally positioned elements increase the overall antenna size up to approximately $4.3\lambda_0$, which can be practically challenging for some applications.

In this paper, a compact singly fed wideband circularly polarized DRA is proposed for 5G applications (3.3–3.8 GHz) in the Republic of Korea. By optimizing the design parameters of the proposed antenna, resonances of cross-ring slot excited DRA, and a dielectric-loaded cross-ring slot antenna can be merged to achieve a wide AR performance and improved impedance bandwidth of 18.7% and 25.9%, respectively. Furthermore, the effects of adhesives on the AR and antenna input impedance of the DRA was investigated, showing deterioration in AR performance. To avoid undesirable use of adhesive, we introduced two small DR posts at the edge to hold it in position without affecting its radiation characteristics. A MIMO array configuration of the proposed DRA incorporating EBG structure is proposed as well. The proposed structure achieved a high diversity gain (DG) and low envelope correlation coefficient (ECC) while maintaining its overall compact size.

This paper is organized as follows; design and simulations of the proposed DRA are presented in Section II. An investigation into the effects of bonding agent is discussed in Section III. Then, the implementation and measurement result of the proposed DRA along with a comparison with the state-of-the-art designs are discussed in Section IV, followed by the EBG unit cell design and MIMO configuration in Section V and VI, respectively, followed by the conclusion.

II. ANTENNA ELEMENT CONFIGURATION

The geometry of the proposed DRA is illustrated in Figure 1, following by its dimensions in Table 1. FR-4 epoxy ($\varepsilon_{rs} = 4.4$) substrate was used with a thickness h of 1.6 mm and size of 46 × 46 mm. A ground plane was placed on top of the

TABLE 1. Geometrical dimensions of the proposed CP-DRA.

Symbol	Value	Symbol	Value	Symbol	Value
$a = b$	18 mm	s	3 mm	w_s	1 mm
d	20 mm	l_1	3.3 mm	l_{st}	7 mm
t	7 mm	l_2	7.38 mm	w_f	3 mm
d_2	12.5 mm	r	2.5 mm		

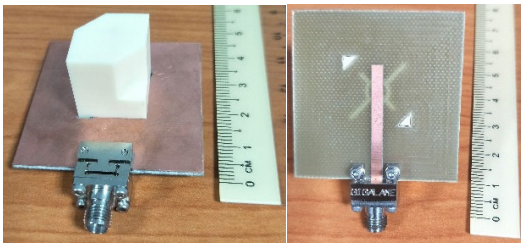

(a) (b)

FIGURE 2. A prototype of the proposed CP-DRA: (a) top and (b) bottom views.

substrate which contained the cross-ring slot with arm lengths l_1 and l_2, slot radius r, and slot width w_s. A rectangular DR of Al_3O_2 material having dimensions of $a \times b \times d$ with $\varepsilon_{rd} = 9.8$ and $\tan\delta = 0.002$ designed using formulas in [34] was placed on top of the cross-ring slot. Furthermore, the DR was truncated in two opposite corners at 45° and depth d_2 and length t. A 50-Ω microstrip feedline of width w_f and stub length l_{st} was printed on the other side of the substrate. Figure 2 illustrates the prototype of the CP-DRA. CP radiation can be achieved by carefully designing the cross-ring slot at an optimal ratio. Initially, the dimensions of the ring can be determined approximately by using the annular slot equation:

$$f_{slot} \approx \frac{c}{2\pi\left(r + \frac{w_s}{2}\right)\sqrt{\varepsilon_{eff}}}, \tag{1}$$

$$\varepsilon_{eff} = \frac{\varepsilon_{rs} + \varepsilon_{rd}}{2}, \tag{2}$$

where c is the speed of light in free space. The dimensions of the inner ring slot of radius r and width w_s were further optimized after including the slot arms with length l_1 and l_2. The slot arms possessing the equal width of the ring slot were placed at 45°, 135°, 225° and 315° on the same plane. Initially, the dimensions of slot arms l_1 and l_2 can be estimated using [3]:

$$2l_1 = 2l_2 = \frac{0.4\lambda_0}{\sqrt{\varepsilon_{eff}}}. \tag{3}$$

Taking note that the ratio of the slot arms l_1/l_2 was set to 2.236 after optimization. Next, the truncation width and depth of dimensions t and d_2 were optimally chosen for the DR to acquire wider CP operation. The right-angled triangular stands were designed with equal side lengths s and substrate thickness h. The simulated minimum ARs resonated at 3.45 GHz and 3.80 GHz.

Figure 3. Shows the electric field distribution of the proposed DRA at 3.45 GHz, which resembles the TE_{111} mode

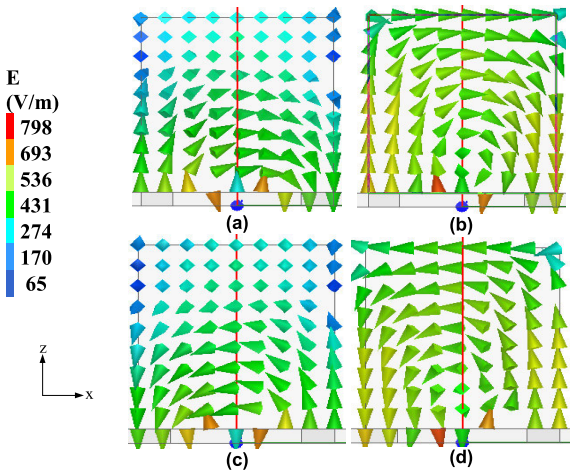

FIGURE 3. E-fields of the proposed DRA excited in the fundamental mode at 3.45 GHz: (a) phase 0°, (b) phase 90°, (c) phase 180° and (d) phase 270°.

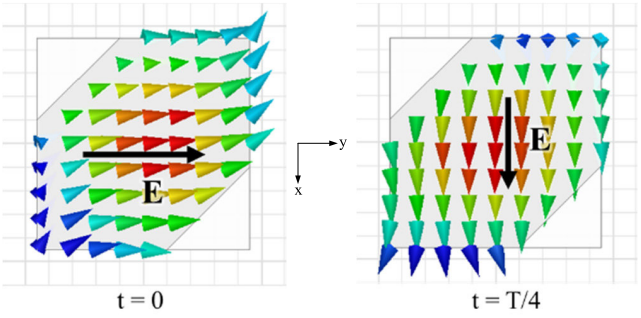

FIGURE 4. E-field distribution at the top of the DR for time period T at 3.45 GHz.

of a regular rectangular DRA. Thus, we call this the quasi-TE_{111} mode. Circular polarization in the proposed antenna was verified by plotting the electric field distribution on the DR at 90° intervals, as shown in Figure 3. Equal electrical field distributions at the most adjacent broadside mode with the quasi-TE_{113} of the DRA was at 5 GHz. The direction of the circular polarization can be determined from the electric field distribution on the top surface of the DR ($\theta = 0°$) at 3.45 GHz, as depicted in Figure 4. For t = 0, vector E points toward the right, while at t = T/4, the vector E electric field rotates 90° in the clockwise direction. The two vectors are orthogonal to each other with a clockwise rotation, thus confirming that the proposed antenna exhibited left-handed circular polarization (LHCP) radiation.

III. EFFECT OF ADHESIVE

Typically, a DR is mounted on a substrate with a feed structure along with the ground plane using an adhesive material. Radiation characteristics such as antenna impedance and quality of polarization are greatly affected by the additional layer of adhesive material, which is predominantly due to a mismatch between the different permittivity of the adhesive layer with nonzero thickness. Therefore, the adhesive material must be precisely accounted for during the design

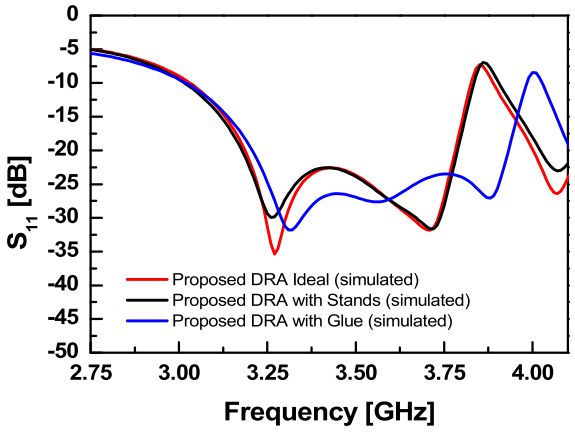

FIGURE 5. Comparison of the reflection coefficients of the proposed DRA mounted using miniature stands and with glue.

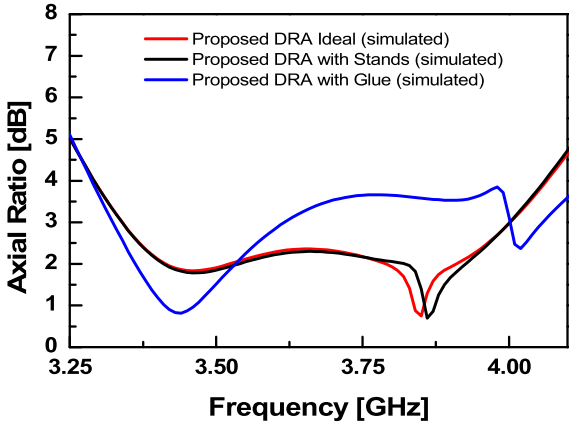

FIGURE 6. Comparison of the AR of the proposed DRA mounted using miniature stands and with glue.

stage to predict the realized DRA performance. With the use of cutting-edge manufacturing technologies, error probability can be reduced by exploiting the fabrication tolerance to its maximum. However, these approaches are generally expensive and cater to bulk production [21].

To gauge the effects of an ordinary adhesive, we compared the reflection coefficient, and AR performance between a DRA mounted with glue and one with the small triangular stands. The simulated reflection coefficient and AR performance are shown in Figure 5 and Figure 6, respectively. For the DRA to be ideally placed on top of the substrate, in which there was no glue or mounting technique applied. In the case of the DRA attached with glue, a layer of glue with an approximated dielectric constant of 3.65 at 3.5 GHz (obtained from the results in [35]) was simulated with a thickness of 0.05 imm. With the applied glue layer, the simulated impedance bandwidth increased from 3.02 to 3.98 GHz while the AR response severely degraded over the designated operation bandwidth, as presented in Figure 5 and Figure 6. The thin layer of glue significantly affected the circular polarization of the antenna due to the additional dielectric permittivity causing changes in radiation characteristics. To avoid performance degradation due to adhesive, we implemented a

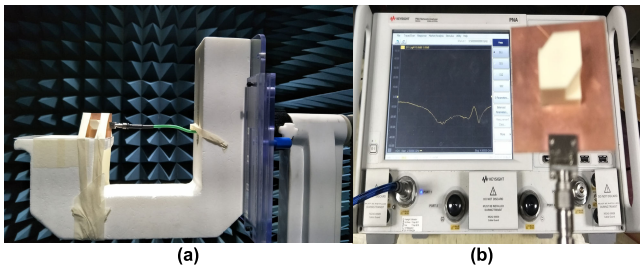

FIGURE 7. Measurement setup for (a) radiation pattern and axial ratio (AR) and (b) antenna input impedance versus frequency.

short triangular post at the bottom of the DR to mechanically attach the DR to the printed circuit board (PCB) without adhesive.

The simulated results of the ideal case without adhesive and the proposed DRA with small stands at the bottom of DR showed no differences in return loss, AR performance, and radiation pattern.

IV. MEASUREMENT RESULTS

The radiation pattern and AR of the proposed DRA were measured in an anechoic chamber at three different frequencies covering the center, lower, and upper frequencies of the entire passband (Figure 7(a)). The chamber was equipped with a near-field scanner and a far-field tower to test and measure the radiation pattern under test. The radiation patterns were measured at 3.45, 3.65, and 3.8 GHz, which covers the lower, upper, and mid frequencies of the desired operation band, respectively. The radiation pattern was measured at each 1-degree step interval in the anechoic chamber having a range of 0–360°. The reflection coefficients of the proposed DRA and the DRA with thin glue layer were measured with N5224A PNA Network Analyzer, as depicted in Figure 7(b).

Figure 8 shows the simulated and measured radiation patterns of the DRA in x-z ($\phi = 90°$) and y-z planes ($\phi = 0°$) at 3.45, 3.65, and 3.80 GHz, respectively. The in the boresight direction, LHCP gain is larger than RHCP by 19, 17 and 18 dB at 3.45, 3.65 and 3.80 GHz, which verifies that the DRA exhibit LHCP radiations. Figure 9 demonstrates the measured and simulated gain plot of the proposed antenna with a measured peak gain of 4.83 dBi within the passband of the antenna. It is known that the measured gain is generally lower than the simulated result due to experiment imperfections such as the losses of connectors and cables are not considered in the far-field measurements. The proposed truncated DRA demonstrates simulated, and measured impedance bandwidths of 23.7% and 25.9% (VSWR = 2:1) within frequency ranges from 3.02 to 3.83 GHz and 3.06 GHz to 3.97 GHz, respectively, as shown in Figure 10. The simulated and measured 3dB AR bandwidths of the antenna were 18.5% (3.34 to 4.02 GHz) and 18.7% (3.15 to 3.80 GHz) in the boresight direction ($\theta = 0°$), as presented in Figure 11. The frequency shifts downward in the AR response of the proposed DRA was due to the incomplete mechanical con-

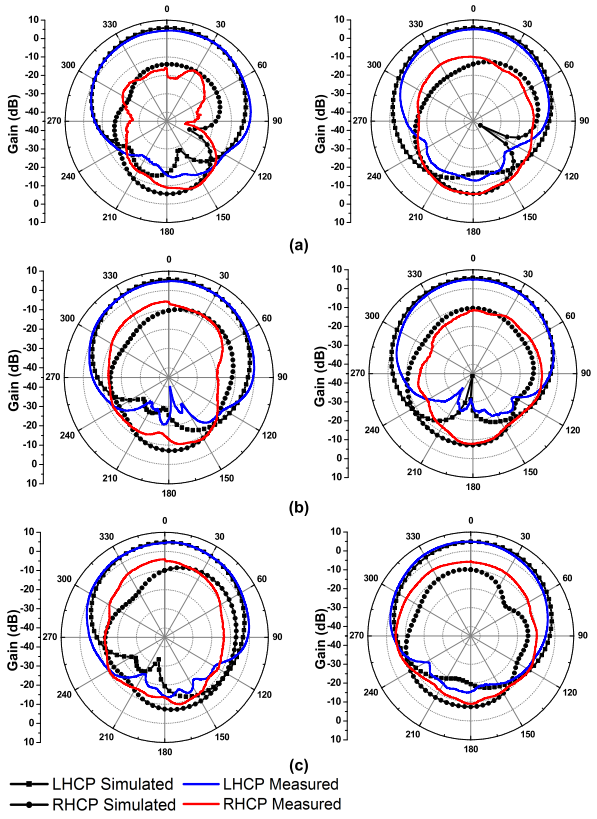

FIGURE 8. Radiation patterns of the proposed DRA at (a) 3.45 GHz, (b) 3.65 GHz and (c) 3.80 GHz (left-hand side images in the x-z plane and right-hand side images in the y-z plane).

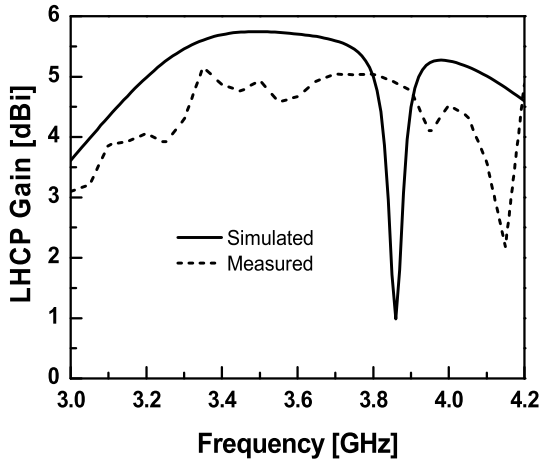

FIGURE 9. Measured and simulated boresight LHCP gain of the proposed antenna.

tact between the conducting parts of the antenna and the DR in this fabrication, resulting in an uneven air gap. It is also noteworthy that the placement and binding support of the DRA during measurement in the chamber contributed toward the effect on the radiation pattern causing a possibly larger AR in the experiment whereas the simulation is always calculated under ideal conditions [36].

The DRA with the applied thin glue layer was also investigated. The simulated and measured impedance bandwidths

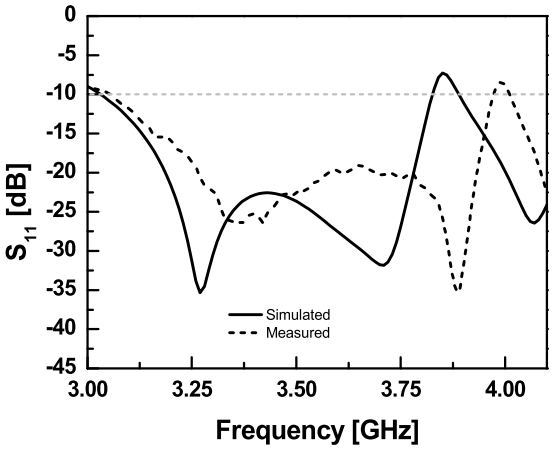

FIGURE 10. Reflection coefficient of the proposed antenna.

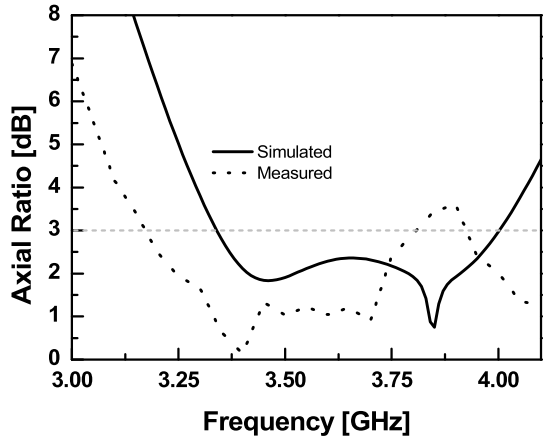

FIGURE 11. Axial ratio of the proposed antenna.

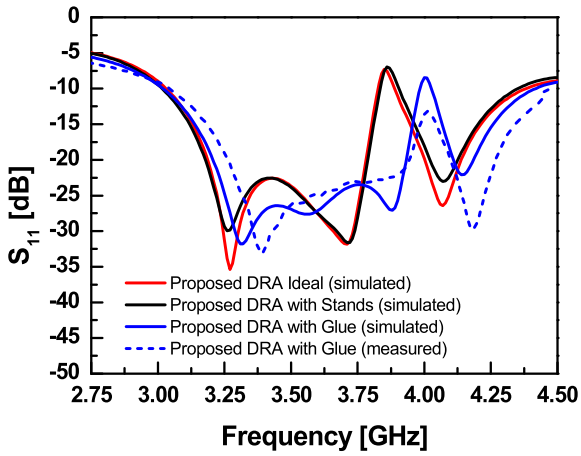

FIGURE 12. Comparison of reflection coefficient for proposed DRA mounted using miniature stands and with glue.

were 27.4% (3.02 to 3.98 GHz) and 30% (3.3 to 4.48 GHz), respectively, as portrayed in Figure 12. The AR response showed a narrow bandwidth of 8% (3.33 to 3.61 GHz) in the simulation and 7% (3.40 to 3.65 GHz) in the experiment, depicted in Figure 13. Table 2 provides a comparison of the proposed CP-DRA and existing singly fed CP-DRAs.

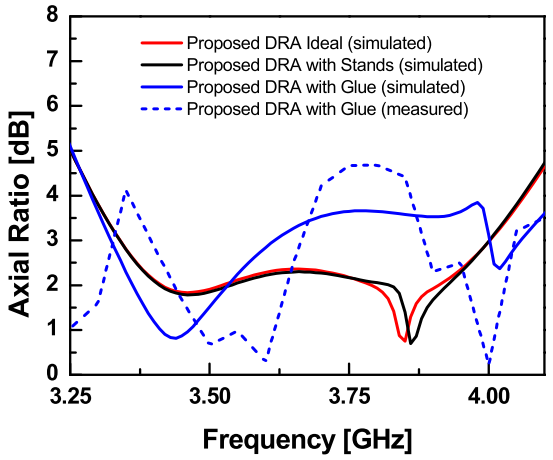

FIGURE 13. Comparison of AR for proposed DRA mounted using miniature stands and with glue.

TABLE 2. Performance comparison of proposed unit DRA design with the state-of-the-art designs in the literature.

Ref.	CP Excitation Method	DR Type	f_0 (GHz)	ε_{rd}	DR Height (mm)	BW_{AR} (%)	LH(RH) CP Gain (dBi)
[8]	Rectangular aperture	Stair-shaped	10	12	0.15 λ_0	10.2	-
[9]	Strips	Hollow Rectangular	2.41	9.4	0.18 λ_0	12.4	6.44
[10]	Spiral strip	Rectangular	4.26	9.3	0.36 λ_0	7	4
[11]	Inclined slots with parasitic strips	Slotted	3.6	15	0.29 λ_0	25	1.48
[12]	Inclined slots with probe	Hollow rectangular	2.5	10	0.26 λ_0	7.3	1.6
[15]	Cross slot fed with cross tuning stub	Rectangular	1.268 & 1.561	20.5	0.23 λ_0	2.9 & 2.4	5.5 & 4.5
[17]	Rectangular slot with DR truncation	Truncation with center groove	1.58 & 2.44	9.8	0.21 λ_0	6.3 & 3.68	6.09 & 8.49
[19]	Circular ring feed with (+)-shaped slot	Rectangular	3.37	9.8	0.20 λ_0	12.03	5
[45]	Modified CPW feed with slotted patches	Half-split cylindrical	4.75	9.8	0.18 λ_0	17.34	1.56
[46]	Concentric parasitic half-loops	Rectangular	3.2	9.2	0.27 λ_0	13	5
[47]	Rectangular slot with Dual-offset feedline	Pixelated	3.2	9.8	0.33 λ_0	14.63	6.13
This Work	**Cross-ring slot with DR truncation**	**Partial truncation**	**3.45**	**9.8**	**0.23 λ_0**	**18.7**	**4.83**

V. MIMO CONFIGURATION

By implementing electromagnetic band-gap (EBG) structure etched onto the ground plane of the MSTL which used in the singly fed DRA, the proposed DRA array can achieve enhanced diversity performance without any extra area consumption required. In this section, geometry and analysis of the MIMO CP-DRA array configuration along with the EBG structure are presented.

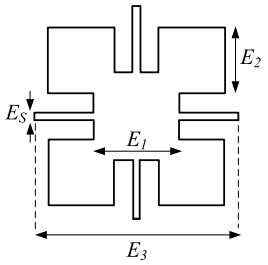

FIGURE 14. EBG unit cell geometry.

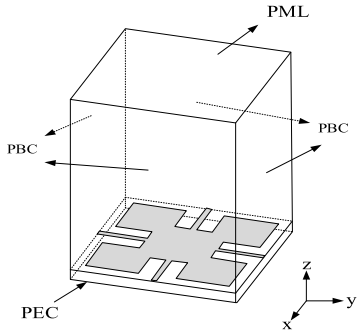

FIGURE 15. Model setup to simulate dispersion diagram in HFSS.

A. ELECTROMAGNETIC BAND-GAP UNIT CELL

Electromagnetic band-gap (EBG) is a periodic structure widely used in microwave circuits, exhibiting frequency zones where surface wave propagation is prohibited [37]. Planar EBGs (without vias), having wide band-gap properties are investigated thoroughly in [38]–[40]. The behavior of the uniplanar compact (UC-EBG) geometry is assessed employing a finite element-based analysis of the unit cell and the extraction of the dispersion diagram. The optimized planar EBG structure can then be used to reduce the mutual coupling of a MIMO antenna array. A 3-D finite element (FEM) code with vector finite elements has been implemented to investigate the EBG dispersion diagram. In HFSS, a single cell is used in computations, while periodic boundary conditions (PBC) at the cell sidewalls are imposed to account for periodicity as demonstrated in Figure 14. The domain is terminated with perfectly matched layers (PML) on top [40]. The optimized parameters of the EBG unit cell are $E_s = 0.572$ mm, $E_1 = 7.592$ mm, $E_2 = 5.73$ mm and $E_3 = 17.735$ mm.

The band-gap of the EBG structure is determined by plotting the dispersion diagram shown in Figure 16, and the band-gap region is defined as a frequency band where no mode is propagated. The range of frequencies of the band-gap of the designed EBG is from 3.36 GHz to 4.43 GHz.

B. CIRCULARLY POLARIZED MIMO DRA

The proposed circularly polarized MIMO DRA utilizing EBG structure designed in the previous section is as shown in Figure 17(a) and the fabricated antenna in Figure 17 (b). The DRAs are placed on the substrate of 95 × 49.7 mm^2. The center-to-center spacing is $\lambda_0/2$, where λ_0 is the wavelength with respect to 3.3 GHz, which is the lowest operating

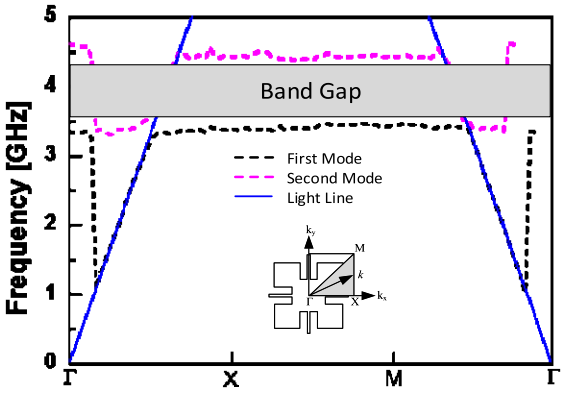

FIGURE 16. Dispersion diagram of EBG unit cell.

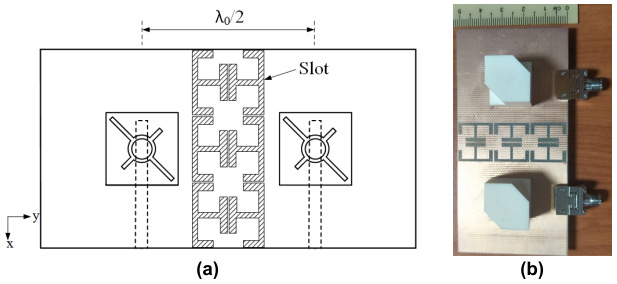

FIGURE 17. (a) Geometry of proposed MIMO DRA (b) Fabricated MIMO CP-DRA.

frequency. The EBG unit cells are engraved onto the ground plane, arranged with first two-unit cells placing at the center with respect to the y-axis, and then extended by half-cell on the top and bottom direction. The positions and alignments are verified through carrying out abundant parametric analysis.

Simulated and measured reflection coefficient, S_{11}, and transmission coefficient, S_{12} are presented in Figure 18 and Figure 19, respectively. Results are compared with an identical MIMO DRA design without EBG structure, labeled as the reference antenna. It can be observed from the proposed design with the simulated and measured S_{11} bandwidth ranging from 3.11 to 3.84 GHz and 3.15 to 3.93 GHz, showing similar frequency response with the single CP-DRA as per Figure 10. Furthermore, isolation below –24 dB from simulation and –26 dB from measurement is achieved frequency band as compared to the reference antenna, with approximately –17 dB. Surface current distribution of the reference and proposed DRA is also compared through HFSS simulation accordingly in Figure 20. The presence of the EBG demonstrated minimization of current flow from DRA 1 to DRA 2 upon excitation on a single CP-DRA. The analysis is performed such that DRA 1 (left side) is excited, and DRA 2 (right side) is terminated by 50-Ω. Wide CP is also maintained as per single DRA element as shown in the AR plot in Figure 21, plotted along with the comparison of with and without EBG structure. Furthermore, simulated antenna gain and radiation pattern are not compromised with the implementation of the EBG structure, as presented in Figure 22, and Figure 23, respectively.

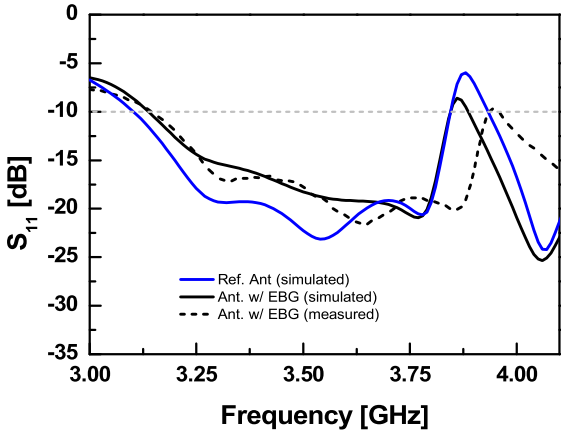

FIGURE 18. Comparison of reflection coefficient for MIMO DRA with and without EBG.

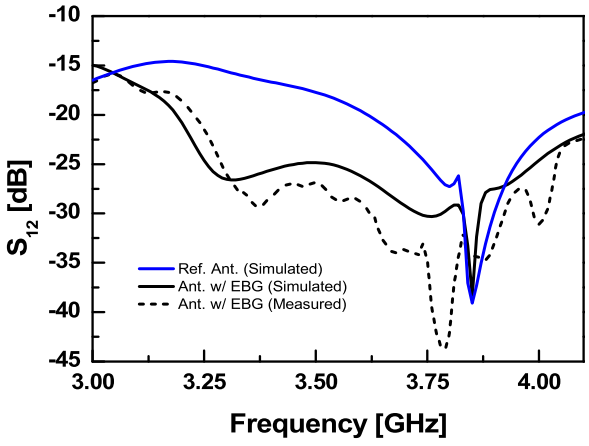

FIGURE 19. Comparison of transmission coefficient for MIMO DRA with and without EBG.

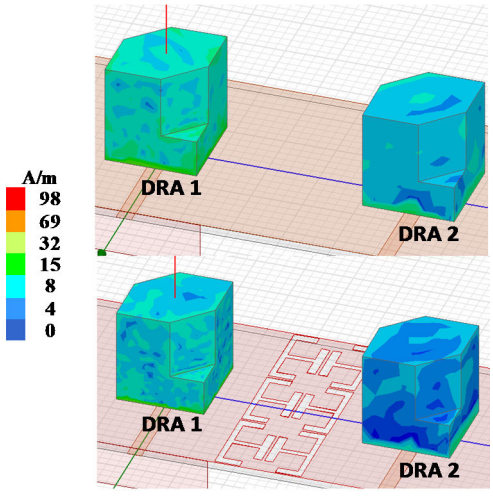

FIGURE 20. Surface current distribution comparison of MIMO DRA with and without EBG.

VI. ANTENNA DIVERSITY ANALYSIS

As destructive interference can take place due to multipath fading, an appropriate antenna diversity scheme can be performed to counter such conditions. The proposed CP MIMO DRA can be evaluated through three essential figures of

TABLE 3. Diversity parameter comparison of the proposed antenna with other CP MIMO DRAs proposed in the literature.

Ref.	Isolation (dB)	ECC	DG (dB)	CCL	Antenna Size (mm^2)
[29]	>18	<0.05	>9.96	NA	0.92 λ_0×0.92 λ_0
[30]	>25	<0.04	>9.16	NA	0.96 λ_0×0.77 λ_0
[31]	>20	<0.10	>8.50	NA	1.04 λ_0×1.62 λ_0
[32]	>18	<0.06	>9.90	<0.23	1.33 λ_0×0.95 λ_0
[33]	> 28	<0.04	>8.00	NA	4.33 λ_0×4.33 λ_0
This Work	**> 26**	**<0.03**	**>9.80**	**<0.10**	**1.09 λ_0× 0.56 λ_0**

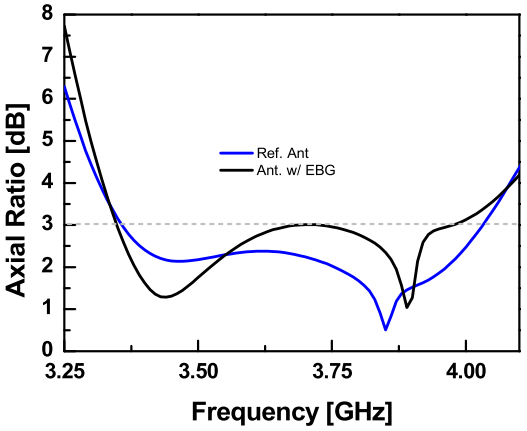

FIGURE 21. AR Comparison of MIMO DRA with and without EBG.

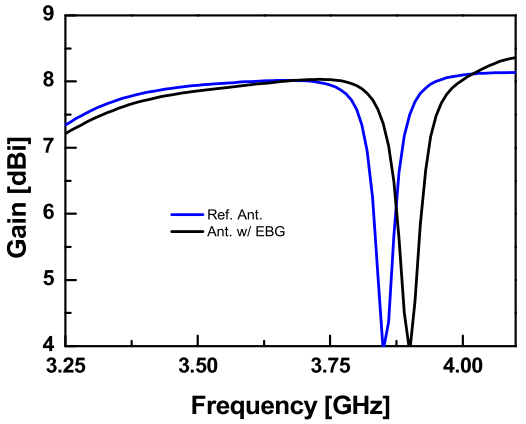

FIGURE 22. Gain comparison of MIMO DRA with and without EBG.

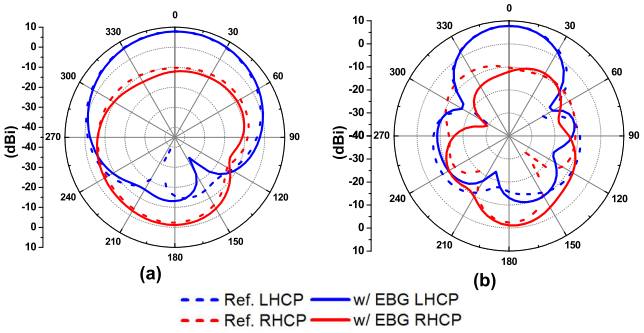

FIGURE 23. Radiation pattern plane for MIMO DRA with and without EBG (a) x-z plane (b) y-z plane.

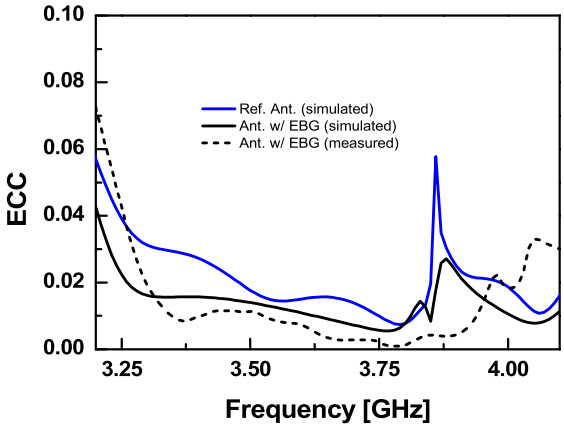

FIGURE 24. Comparison of envelope correlation coefficients (ECCs) for the antenna with and without EBG.

merit, namely envelope correlation coefficient (ECC), diversity gain (DG) and channel capacity loss (CCL) [41]–[44] for its diversity performance. Comparison between the state-of-the-art MIMO CP-DRAs is also carried out, as shown in Table 3.

A. ENVELOPE CORRELATION COEFFICIENT

The performance of MIMO DRAs is measured using the envelope correlation coefficient (ECC). The ECC measures the similarity between two antennas' radiation patterns.

Considering an ideal case when ECC = 0, two radiation patterns are not overlapped, the incoming signal is received by a single array element from any direction. In contrast, when ECC = 1, two radiation patterns are identical. The signal will be equally received by both ports in this case, which is undesirable. ECC of lower values is generally preferred, whereby values of below 0.5 is considered acceptable. The ECC can be calculated using the equation in [41]:

$$ECC = \rho_e = \frac{|S_{ii}^* S_{ij} + S_{ji}^* S_{jj}|^2}{\left[1 - (|S_{ii}|^2 + |S_{ji}|^2)\right]\left[1 - (|S_{jj}|^2 + |S_{ij}|^2)\right]} \quad (4)$$

The simulated ECCs for the reference antenna and the proposed antenna is compared, as shown in Figure 24. The proposed antenna achieved a simulated and measured ECC of below 0.02 throughout the entire band. Whereas the ECC of the reference antenna with EBG became larger than 0.03 from 3.3 GHz.

B. DIVERSITY GAIN

Diversity gain (DG) is another essential parameter used to validate the performance of MIMO antennas. The approximate relationship between ECC and DG is presented in [42]:

$$DG = 10 \times \sqrt{1 - |ECC|} \quad (5)$$

DG value of 10 is considered ideal; however, above 6 is within a suitable level [43]. As shown in Figure 25, the DG of the proposed antenna is above 9.8 within the band of operation.

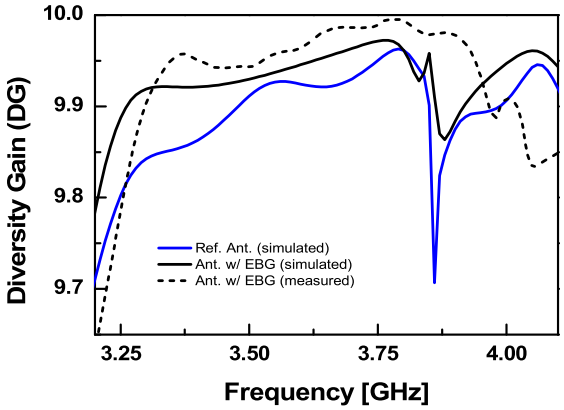

FIGURE 25. Comparison of diversity gain (DG) for antenna with and without EBG.

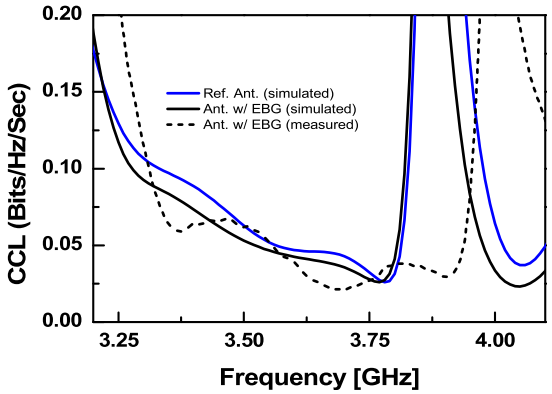

FIGURE 26. Comparison of channel capacity loss (CCL) for antenna with and without EBG.

C. CHANNEL CAPACITY LOSS

Channel capacity loss (CCL) is generally affected by the coupling between numerous antennas, whereby CCL increases proportionally with the number of antenna elements. As the correlation between array elements in a MIMO channel generates CCL, it can be calculated as below [44]:

$$CCL = -\log_2 \det\left(\psi^R\right) \tag{6}$$

$$\psi^R = \begin{bmatrix} \rho_{11} & \rho_{12} \\ \rho_{21} & \rho_{22} \end{bmatrix} \tag{7}$$

$$\rho_{ii} = 1 - \left(\left|S_{ii}\right|^2 + \left|S_{ij}\right|^2\right) \tag{8}$$

$$\rho_{ij} = -\left(S_{ii}^* \times S_{ij} + S_{ji}^* \times S_{jj}\right), \quad i \text{ and } j = 1 \text{ or } 2 \tag{9}$$

Compared to the reference antenna, there is a slight frequency shift in the CCL of the proposed MIMO DRA, hence showing no significant difference at the intercepting point at 3.5 GHz. However, the proposed antenna still demonstrates a response below 0.1 bits/Hz/sec over the desired passband, as presented in Figure 25.

VII. CONCLUSION

A wideband CP-DRA is proposed in this paper. To achieve a wideband AR performance, we applied 45° partial truncation at two opposite corners of the DR combined with a cross-ring coupling slot with an optimum ratio. The effect of the adhesive used for attaching the DR to the PCB with the coupling feeding structure was investigated, and the measurements showed that it severely degraded the 3-dB bandwidth of the AR. Small triangular stands were implemented at the bottom of the DR to mount it on the PCB, which avoided any adverse effects. The proposed antenna demonstrated the measured impedance and AR bandwidths of 25.9% and 18.7%, respectively, which fully supports the frequency range of 5G application systems (3.3–3.8 GHz) in the Republic of Korea. On top of that, the MIMO array configuration with EBG structure was implemented and showed promising isolation performance of –26 dB while maintaining its compact size. The antenna is further verified with the diversity analysis of ECC, DG, and CCL.

REFERENCES

[1] S. Long, M. McAllister, and L. C. Shen, "The resonant cylindrical dielectric cavity antenna," *IEEE Trans. Antennas Propag.*, vol. 31, no. 3, pp. 406–412, May 1983.
[2] K. M. Luk and K. W. Leung, Eds., *Dielectric Resonator Antennas*. Baldock, U.K.: Research Studies, 2003.
[3] A. Petosa, *Dielectric Resonator Antenna Handbook*. Norwood, MA, USA: Artech House, 2007.
[4] R. K. Mongia and P. Bhartia, "Dielectric resonator antennas—A review and general design relations for resonant frequency and bandwidth," *Int. J. Microw. Millim.-Wave Comput. Aided Eng.*, vol. 4, no. 3, pp. 230–247, Jul. 1994.
[5] K. W. Leung, E. H. Lim, and X. S. Fang, "Dielectric resonator antennas: From the basic to the aesthetic," *Proc. IEEE*, vol. 100, no. 7, pp. 2181–2193, Jul. 2012.
[6] G. Massie, M. Caillet, M. Clenet, and Y. M. M. Antar, "A new wideband circularly polarized hybrid dielectric resonator antenna," *IEEE Antennas Wireless Propag. Lett.*, vol. 9, pp. 347–350, 2010.
[7] Y. Pan, K. W. Leung, and E. H. Lim, "Compact wideband circularly polarized rectangular dielectric resonator antenna with dual underlaid hybrid couplers," *Microw. Opt. Technol. Lett.*, vol. 52, no. 12, pp. 2789–2791, Dec. 2010.
[8] R. Chair, S. L. S. Yang, A. A. Kishk, K. F. Lee, and K. M. Luk, "Aperture fed wideband circularly polarized rectangular stair shaped dielectric resonator antenna," *IEEE Trans. Antennas Propag.*, vol. 54, no. 4, pp. 1350–1352, Apr. 2006.
[9] M. I. Sulaiman and S. K. Khamas, "A singly fed rectangular dielectric resonator antenna with a wideband circular polarization," *IEEE Antennas Wireless Propag. Lett.*, vol. 9, pp. 615–618, 2010.
[10] K. Lu, K. W. Leung, and Y. M. Pan, "Theory and experiment of the hollow rectangular dielectric resonator antenna," *IEEE Antennas Wireless Propag. Lett.*, vol. 10, pp. 631–634, 2011.
[11] Y. M. Pan and K. W. Leung, "Wideband omnidirectional circularly polarized dielectric resonator antenna with parasitic strips," *IEEE Trans. Antennas Propag.*, vol. 60, no. 6, pp. 2992–2997, Jun. 2012.
[12] Y. M. Pan, K. W. Leung, and K. Lu, "Omnidirectional linearly and circularly polarized rectangular dielectric resonator antennas," *IEEE Trans. Antennas Propag.*, vol. 60, no. 2, pp. 751–759, Feb. 2012.
[13] M. Khalily, M. R. Kamarudin, and M. H. Jamaluddin, "A novel square dielectric resonator antenna with two unequal inclined slits for wideband circular polarization," *IEEE Antennas Wireless Propag. Lett.*, vol. 12, pp. 1256–1259, Sep. 2013.
[14] A. Buerkle, K. Sarabandi, and H. Mosallaei, "Compact slot and dielectric resonator antenna with dual-resonance, broadband characteristics," *IEEE Trans. Antennas Propag.*, vol. 53, no. 3, pp. 1020–1027, Mar. 2005.
[15] X.-C. Wang, L. Sun, X.-L. Lu, S. Liang, and W.-Z. Lu, "Single-feed dual-band circularly polarized dielectric resonator antenna for CNSS applications," *IEEE Trans. Antennas Propag.*, vol. 65, no. 8, pp. 4283–4287, Aug. 2017.
[16] J. Pan and M. Zou, "Wideband hybrid circularly polarised rectangular dielectric resonator antenna excited by modified cross-slot," *Electron. Lett.*, vol. 50, no. 16, pp. 1123–1125, Jul. 2014.
[17] X. Fang, K. W. Leung, and E. H. Lim, "Singly-fed dual-band circularly polarized dielectric resonator antenna," *IEEE Antennas Wireless Propag. Lett.*, vol. 13, pp. 995–998, 2014.

[18] N. Yang, K. W. Leung, K. Lu, and N. Wu, "Omnidirectional circularly polarized dielectric resonator antenna with logarithmic spiral slots in the ground," *IEEE Trans. Antennas Propag.*, vol. 65, no. 2, pp. 839–844, Feb. 2017.
[19] R. Kumar and R. K. Chaudhary, "Circularly polarized rectangular DRA coupled through orthogonal slot excited with microstrip circular ring feeding structure for Wi-MAX applications," *Int. J. RF Microw. Comput. Aided Eng.*, vol. 28, Jan. 2018, Art. no. e21153.
[20] A. M. Faiz, N. Gogosh, S. A. Khan, and M. F. Shafique, "Effects of an ordinary adhesive material on radiation characteristics of a dielectric resonator antenna," *Microw. Opt. Technol. Lett.*, vol. 56, no. 6, pp. 1502–1506, Jun. 2014.
[21] C. Sarkar, D. Guha, and C. Kumar, "Glueless compound ground technique for dielectric resonator antenna and arrays," *IEEE Antennas Wireless Propag. Lett.*, vol. 16, pp. 2440–2443, 2017.
[22] X. Chen, S. Zhang, and Q. Li, "A review of mutual coupling in MIMO systems," *IEEE Access*, vol. 6, pp. 24706–24719, 2018.
[23] M. S. Sharawi, A. B. Numan, and D. N. Aloi, "Isolation improvement in a dual-band dual-element MIMO antenna system using capacitively loaded loops," *Prog. Electromagn. Res.*, vol. 134, pp. 247–266, 2013.
[24] K. Trivedi and D. Pujara, "Mutual coupling reduction in wideband tree shaped fractal dielectric resonator antenna array using defected ground structure for MIMO applications," *Microw. Opt. Technol. Lett.*, vol. 59, no. 11, pp. 2735–2742, Nov. 2017.
[25] K. Trivedi and D. Pujara, "Mutual coupling reduction in UWB modified maltese shaped DRA array for MIMO applications," in *Proc. 48th Eur. Microw. Conf. (EuMC)*, Madrid, Spain, Sep. 2018, pp. 1117–1120.
[26] M. J. Al-Hasan, T. A. Denidni, and A. R. Sebak, "Millimeter-wave compact EBG structure for mutual coupling reduction applications," *IEEE Trans. Antennas Propag.*, vol. 63, no. 2, pp. 823–828, Feb. 2015.
[27] A. Dadgarpour, B. Zarghooni, B. S. Virdee, T. A. Denidni, and A. A. Kishk, "Mutual coupling reduction in dielectric resonator antennas using metasurface shield for 60-GHz MIMO systems," *IEEE Antennas Wireless Propag. Lett.*, vol. 16, pp. 477–480, 2017.
[28] M. Farahani, J. Pourahmadazar, M. Akbari, M. Nedil, A. R. Sebak, and T. A. Denidni, "Mutual coupling reduction in millimeter-wave MIMO antenna array using a metamaterial polarization-rotator wall," *IEEE Antennas Wireless Propag. Lett.*, vol. 16, pp. 2324–2327, 2017.
[29] N. K. Sahu, K. Das, and R. K. Gangwar, "Dielectric resonator-based wide band circularly polarized MIMO antenna with pattern diversity for WLAN applications," *Microw. Opt. Technol. Lett.*, vol. 60, no. 12, pp. 2855–2862, Dec. 2018.
[30] G. Das, A. Sharma, and R. K. Gangwar, "Dielectric resonator based circularly polarized MIMO antenna with polarization diversity," *Microw. Opt. Technol. Lett.*, vol. 60, no. 3, pp. 685–693, Mar. 2018.
[31] A. Sharma, G. Das, and R. K. Gangwar, "Dual polarized triple band hybrid MIMO cylindrical dielectric resonator antenna for LTE2500/WLAN/WiMAX applications," *Int. J. RF Microw. Comput. Aided Eng.*, vol. 26, no. 9, pp. 763–772, Nov. 2016.
[32] N. K. Sahu, G. Das, and R. K. Gangwar, "Dual polarized triple-band dielectric resonator based hybrid MIMO antenna for WLAN/WiMAX applications," *Microw. Opt. Technol. Lett.*, vol. 60, no. 4, pp. 1033–1041, Apr. 2018.
[33] J. Iqbal, U. Illahi, M. I. Sulaiman, M. M. Alam, M. M. Su'ud, and M. N. Mohd Yasin, "Mutual coupling reduction using hybrid technique in wideband circularly polarized MIMO antenna for WiMAX applications," *IEEE Access*, vol. 7, pp. 40951–40958, 2019.
[34] X. S. Fang and K. W. Leung, "Designs of single-, dual-, wide-band rectangular dielectric resonator antennas," *IEEE Trans. Antennas Propag.*, vol. 59, no. 6, pp. 2409–2414, Jun. 2011.
[35] A. Rashidian, L. Shafai, and D. M. Klymyshyn, "Compact wideband multimode dielectric resonator antennas fed with parallel standing strips," *IEEE Trans. Antennas Propag.*, vol. 60, no. 11, pp. 5021–5031, Nov. 2012.
[36] J. Y. Yin, X. Wan, J. Ren, and T. J. Cui, "A circular polarizer with beamforming feature based on frequency selective surfaces," *Sci. Rep.*, vol. 7, Jan. 2017, Art. no. 41505.
[37] F. Yang and Y. Rahmat-Samii, *Electromagnetic Band Gap Structures in Antenna Engineering*. Cambridge, U.K.: Cambridge Univ. Press, 2009.
[38] R. Coccioli, F.-R. Yang, K.-P. Ma, and T. Itoh, "Aperture-coupled patch antenna on UC-PBG substrate," *IEEE Trans. Microw. Theory Techn.*, vol. 47, no. 11, pp. 2123–2130, Nov. 1999.
[39] E. Rajo-Iglesias, Ó. Quevedo-Teruel, and L. Inclan-Sanchez, "Mutual coupling reduction in patch antenna arrays by using a planar EBG structure and a multilayer dielectric substrate," *IEEE Trans. Antennas Propag.*, vol. 56, no. 6, pp. 1648–1655, Jun. 2008.
[40] S. D. Assimonis, T. V. Yioultsis, and C. S. Antonopoulos, "Computational investigation and design of planar EBG structures for coupling reduction in antenna applications," *IEEE Trans. Magn.*, vol. 48, no. 2, pp. 771–774, Feb. 2012.
[41] S. Blanch, J. Romeu, and I. Corbella, "Exact representation of antenna system diversity performance from input parameter description," *Electron. Lett.*, vol. 39, no. 9, pp. 705–707, May 2003.
[42] K. Rosengren and P.-S. Kildal, "Radiation efficiency, correlation, diversity gain and capacity of a six-monopole antenna array for a MIMO system: Theory, simulation and measurement in reverberation chamber," *IEE Proc.-Microw., Antennas Propag.*, vol. 152, no. 1, pp. 7–16, 2005.
[43] A. Iqbal, O. A. Saraereh, A. W. Ahmad, and S. Bashir, "Mutual coupling reduction using F-shaped stubs in UWB-MIMO antenna," *IEEE Access*, vol. 6, pp. 2755–2759, 2018.
[44] S. H. Chae, S.-K. Oh, and S.-O. Park, "Analysis of mutual coupling, correlations, and TARC in WiBro MIMO array antenna," *IEEE Antennas Wireless Propag. Lett.*, vol. 6, pp. 122–125, 2007.
[45] R. Kumar and R. K. Chaudhary, "A new modified CPW-fed wideband circularly polarized half-split cylindrical dielectric resonator antenna with different permittivity of two layers in radial direction," *Int. J. RF Microw. Comput.-Aided Eng.*, vol. 27, no. 3, Mar. 2017, Art. no. e21068.
[46] M. I. Sulaiman and S. K. Khamas, "A singly fed wideband circularly polarized dielectric resonator antenna using concentric open half-loops," *IEEE Antennas Wireless Propag. Lett.*, vol. 10, pp. 1305–1308, Nov. 2011.
[47] S. Trinh-Van, Y. Yang, K.-Y. Lee, and K. C. Hwang, "A wideband circularly polarized pixelated dielectric resonator antenna," *Sensors*, vol. 16, no. 9, p. 1349, Sep. 2016.

HSIANG NERNG CHEN received the B.E. degree in telecommunication engineering from the Asia Pacific University of Technology and Innovation, Kuala Lumpur, Malaysia, in 2016. He is currently pursuing the master's degree in electronics and electrical engineering with Dongguk University, Seoul, South Korea.

His current research interests include microstrip patch antennas and dielectric resonator antennas.

JEONG-MOON SONG received the B.Sc. degree from Dongguk University, Seoul, South Korea, in 2019, where he is currently pursuing the master's degree in electronics and electrical engineering.

His current research interests include dielectric resonator antennas and antenna measurements.

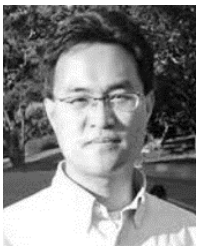

JUNG-DONG PARK (M'15–SM'18) received the B.Sc. degree from Dongguk University, Seoul, South Korea, in 1998, the master's degree from the Gwangju Institute of Science and Technology (GIST), Gwangju, South Korea, in 2000, and the Ph.D. degree in EECS from the University of California at Berkeley, Berkeley, CA, USA, in 2012.

From 2000 to 2002, he was with the Institute for Advanced Engineering (IAE), Yongin, South Korea, where he was involved in the design of 35-GHz radar/radiometer transceivers. From 2002 to 2007, he was a Senior Researcher with the Agency for Defense Development (ADD), Daejeon, South Korea, where he was responsible for the development of millimeter-wave (mmW) passive/active sensors and related mmW modules. From 2007 to 2012, he was with the Berkeley Wireless Research Center (BWRC), where he worked on silicon-based RF/millimeter-wave/terahertz antennas, circuits, and systems. From 2012 to 2015, he was with Qualcomm Inc., San Jose, CA, USA. He is currently an Associate Professor with the Division of Electronics and Electrical Engineering, Dongguk University. His research interests include wireless and broadband communications and remote sensors, analog, RFICs, various antennas, and microwave electronics.